

We are IntechOpen, the world's leading publisher of Open Access books Built by scientists, for scientists

6,900

Open access books available

186,000

International authors and editors

200M

Downloads

Our authors are among the

154

Countries delivered to

TOP 1%

most cited scientists

12.2%

Contributors from top 500 universities



WEB OF SCIENCE™

Selection of our books indexed in the Book Citation Index
in Web of Science™ Core Collection (BKCI)

Interested in publishing with us?
Contact book.department@intechopen.com

Numbers displayed above are based on latest data collected.
For more information visit www.intechopen.com



Multilayered Solar Energy Converters with Flexible Sequence of p and n Semiconductor Films

Yuri V. Vorobiev, Iker R. Chávez Urbiola,
Rafael Ramírez Bon, Liliana Licea Jiménez,
Sergio A. Pérez García, Pavel Vorobiev and
Paul Horley

Additional information is available at the end of the chapter

<http://dx.doi.org/10.5772/65013>

Abstract

Non-traditional design of multi-layered solar energy converters is proposed, with electrically independent p - i - n junctions. This new approach allows utilization of cheap and abundant II-VI, IV and IV-VI materials instead of III-V ones, using also cheap and economic deposition techniques like Chemical Bath Deposition (CBD) or Chemical Vapor Deposition (CVD) instead of expensive Molecular Beam Epitaxy (MBE). The CVD reactor with three atomic sources was built and used. II-VI and IV-VI semiconductor materials were prepared either in CVD reactor, or by CBD techniques. Besides, the original two-stage technology was employed: first the precursor oxide/hydroxide film of corresponding metal (like cadmium oxide/hydroxide) was prepared by some variety of CBD methods, and at the second stage, in CVD reactor the non-metallic component of precursor film was substituted by chalcogen, producing materials like CdS, CdSe, PbTe, etc. The semiconductor materials thus produced were of high quality, with basic parameters corresponding to those for the single crystals. Several experimental multilayered converters were constructed (in particular, with CdS/CdTe, CdS/PbS and Si/PbTe active bilayers). The preliminary results of their studying have shown that these and similar devices can be used in solar cells and photo sensors with satisfactory efficiency, and have great potential for improvement.

Keywords: multilayered solar cells, independent p - n junctions, II-VI and IV-VI semiconductor films, chemical bath deposition, chemical vapor deposition

1. Introduction

To utilize efficiently, a wide solar spectrum in conversion of solar radiation to electricity, several semiconductors with different band gaps must be used. This is usually realized in tandem solar energy converters with 2–4 *p-i-n* junctions of different semiconductors connected in series [1–3]. This design is applied to the solar cells made of different materials, including amorphous and organic ones. However, in the most efficient tandem converters (like those used in space applications), the expensive III–V materials are usually used, with molecular beam epitaxy (MBE) deposition technique that is also expensive. Besides, the serial connection of the elements means that the least effective junction defines the total photo current generated; the tunneling between adjacent *p-i-n* junctions causes additional losses.

Recently, we proposed a different construction of solar energy converters based on two of our patents [4–6], with electrically independent junctions that allow having a flexible sequence of *p* and *n* layers in them, and physically separate several junctions. This approach brings additional degrees of freedom to the converter's design, reduces the losses due to tunneling among the junctions and allows utilization of essentially cheaper II–VI, IV and IV–VI materials instead of III–V ones, with simple, cheap and ecologically pure technologies such as chemical bath deposition (CBD) with its variations (photo chemical bath deposition (PCBD) and successive ionic layer adsorption and reaction (SILAR)) or chemical vapor deposition (CVD), preserving high efficiency of solar energy conversion. This approach is explained in detail below, and the corresponding preliminary experimental results are presented.

2. Tandem solar cells—advantages and shortcomings: revision of the classical architecture

The first solar cell (1954) had the efficiency of 6%; today, after more than 60 years of research and development, the commercial solar modules reach efficiencies of 10–15%. This small value is a consequence of a wide solar spectrum, so that photons with maximum energy of 3–4 eV being absorbed in a semiconductor cell's material (Si, for example, with a band gap of around 1 eV) produce one electron-hole pair separated after thermalization in energy scale by this 1 eV, and the difference between the photon's energy and the band gap value is quickly (at approximately 10^{-12} s) transformed to heat by the process of emission of phonons. On the other hand, photons with energy smaller than the band gap are not absorbed and thus lost for energy conversion. Consequently, even in an ideal case when no other losses are present, the efficiency of one-semiconductor solar cell is not larger than approximately 30% (the so-called Schokley-Queisser limit [7]), and the corresponding practical limit is around 15%.

To achieve a higher efficiency of solar energy conversion, the abovementioned tandem photovoltaic converters are used, which actually are serially connected *p-i-n* junctions of different semiconductor materials with gradually decreasing band gap, such as GaAs-Ge, InGaP-GaAs-Ge [8] or InGaAsN-GaAs-InGaAlP [9], so that each junction absorbs a part of

solar spectrum with photons larger than its band gap, transmitting the rest of the spectrum to the next junction. The record efficiency of such a tandem is around 40%, with the price higher than that of conventional solar modules by orders of magnitude: that is why they are used mainly in satellites, and their production [8] is closely related to satellite industry.

The high cost of production of the classic tandem cells is an evident consequence of the necessity of a very precise design of each of the constituent $p-i-n$ junctions, in a sense that each one must generate the same photocurrent on absorbing of the corresponding part of solar spectrum, because of their serial connection. To fulfill this condition, a strict control of the deposition process is needed (expensive MBA equipment), together with expensive III-V semiconductor materials. We believe that following this route, it will be impossible to create efficient and economic solar energy converter for terrestrial applications.

2.1. Multi-junction solar energy converters with electrically independent $p-i-n$ junctions

Our approach is based upon the elimination of serial connection of the $p-i-n$ junctions in a tandem, making them electrically independent, with the idea that if the tandem is not working alone (reasonable assumption in case of mass application), it is always possible to find an optimum connection of constituents even if they do not generate the same current thus evading the main restriction of the classical tandem. At that, the device can be monolithic or have physically separated parts; we are not proposing stack of separate cells (see, for example, [10]).

Thus, we suggest [4–6] that each semiconductor $p-i-n$ junction in the converter has electric contacts at both ends, and to make its parts electrically independent, an insulating layer can be introduced between the parts; we shall see that it will not always be necessary. The simplest case is a two-junction device, presented in **Figure 1** (left part—the device construction scheme; right part—scheme of energy bands). We stress that in this case, no tunnel junction exists in the device, which gives additional advantage over the classical tandem.

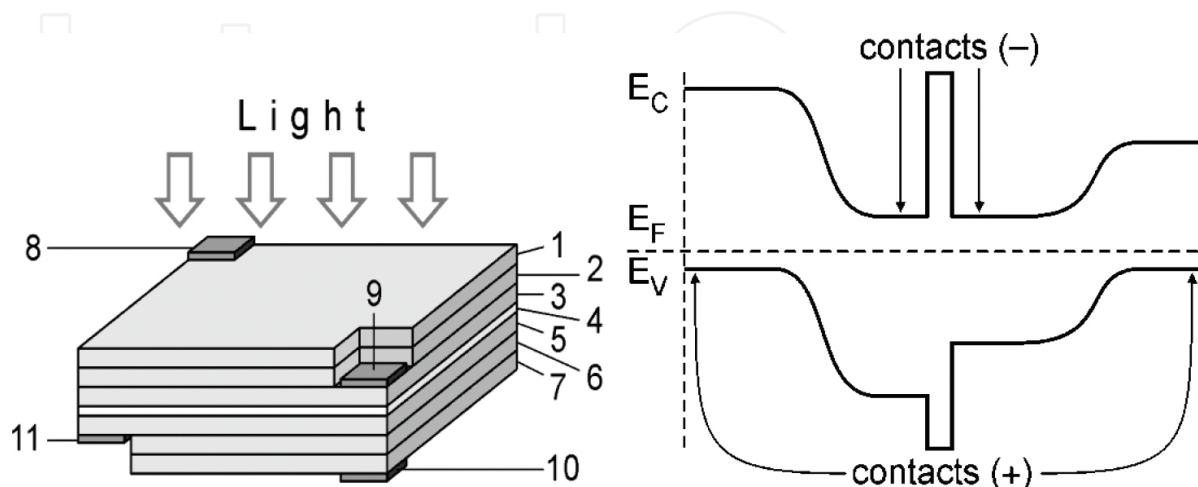


Figure 1. Construction scheme (left) and energy band diagram (right) of a two-junction device.

As illustrated in **Figure 1**, the two-junction version of our solar energy converter includes the two $p-i-n$ junctions of the semiconductor materials having different band gap values. The top cell has a « $p-i-n$ » sequence of layers; the bottom cell has a « $n-i-p$ » sequence, with an insulating layer between the two active cells.

The top cell comprises the p -layer 1, the i -layer 2 and the n -layer 3. After the insulating layer 4 follows the n -layer of the bottom cell 5, then the i -layer 6 and the p -layer 7. The top contact 8 to the upper p -layer 1 of the top cell serves for electrical connections; the transparent conductive layer (or heavily doped one) can be introduced between the p -layer 1 and the contact 8 (not shown in the figure); 9 is the electric contact to the n -layer 3 of the top cell; 11 is the electric contact to the n -layer 5 of the bottom cell, and 10 is the electric contact to the p -layer 7 of the bottom cell. Again, the contacts 9–11 can be added with the transparent conductive layer on the surface of the corresponding semiconductor layer.

The possible ways of the electrical connections of the contacts are shown in **Figure 2**. **Figure 2A** refers to the case when there is only one working two-junction device of the present type. Since the two cells, as a rule, generate the different photo voltage (the larger is the band gap, the larger the potential barrier, and the larger voltage), the only possible way of connection is in series, which is illustrated by the **Figure 2A**: the negative contact of one cell is connected to the positive contact of the other one, and the other two contacts are used to connect the device into external circuit.

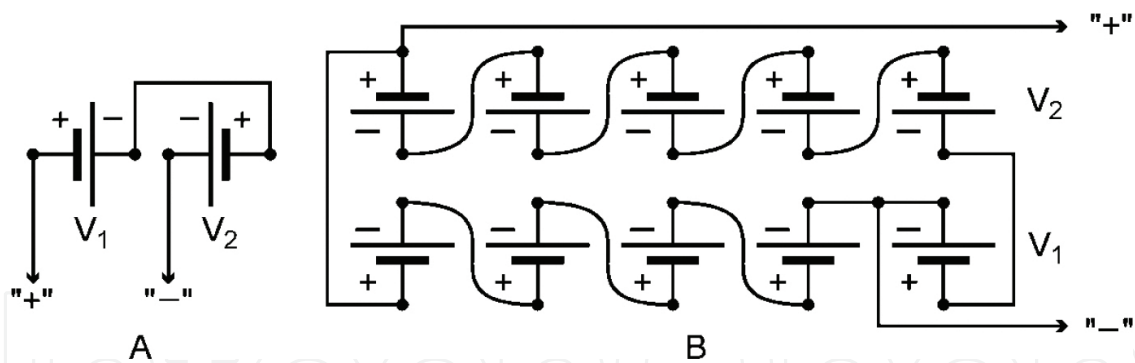


Figure 2. Electrical connections among device's elements (see text for the details).

When several devices of this type are working (in a solar module), there are many options of connection, which might be chosen to provide the necessary voltage of the module. **Figure 2B** gives an example of the cells' interconnection in a module consisting of five two-junction converters of the present type, corresponding to the case, when the photo voltage of the top cell is $V_1 = 1.55$ V and the photo voltage of the bottom cell is $V_2 = 0.93$ V. All five bottom cells and one of the top cells are connected in series producing the voltage $5V_2 + V_1 = 6.2$ V; the other four top cells connected in series produce the same voltage: $4V_1 = 6.2$ V. These two arrays must be connected in parallel, to double the photo current. For a larger amount of the devices in a module, there will be more options in electrical connections.

It is evident that the order of semiconductor layers can be reversed (i.e., the device of the type $(n-i-p)_1$ -insulating layer- $(p-i-n)_2$ can be formed, with the same characteristics but the opposite charge on the contacts compared to the case described).

To reduce the solar light reflection at the surface, the antireflection layer might be added to the top cell. In this respect, the multi-junction device of our type is not different from the traditional multi-junction devices. To reduce the reflection losses at the interface between semiconductor and insulating layer, the latter layer's material should have relatively large refractive index N . For example, with the insulating layer of TiO_2 ($N = 2.5$) and semiconductor of GaAs type ($N = 3.5$), the interface reflection coefficient will be less than 3%. For this approximate estimation, we use the Fresnel formula for reflection coefficient at normal incidence

$$R = \left(\frac{\frac{N_2}{N_1} - 1}{\frac{N_2}{N_1} + 1} \right)^2 \quad (1)$$

where N_2 and N_1 are the refractive indices of the materials on two sides of an optical interface (as it is seen from the formula, the order of layers does not affect the reflection coefficient).

Having smaller losses than the traditional two-junction solar energy converter (no tunnel junctions), our device is capable to have higher efficiency and has more options for optimization.

For our version of the three-junction converter, we present the equilibrium energy band diagram in **Figure 3** (left, here the three cells are denoted by numbers I, II and III from left to right).

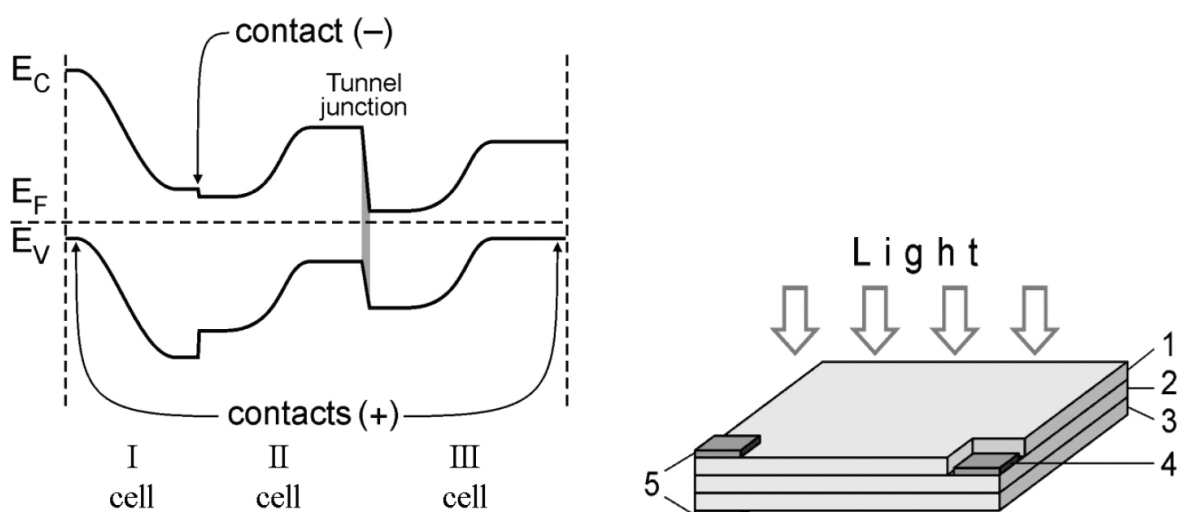


Figure 3. Energy band diagram (left) and construction scheme (right) of three-junction device.

This is a special case, when no insulating layer is needed: The two cells with the larger band gaps both have n -layers at the boundary where the electrode is needed and not the insulator; besides, there is only one tunnel junction instead of two in the traditional three-junction tandem. The device has only three contacts (less than in our two-junction device); the band gaps of the three semiconductor materials are again chosen to utilize in an optimal way the solar spectrum: Here, we must have approximately equal numbers of photons absorbed by the second and the third cells (counting from left to right) which are internally connected in series, but there is no need to have the same photon numbers (i.e., the same photo current) in the first cell.

The sequence of layers from the top to the bottom is as follows: $(p-i-n)_1-(n-i-p)_2-(n-i-p)_3$. One comment in relation to the choice of the type of material and the doping level of semiconductor layers: It has to make the photo voltage of the first cell approximately equal to the summary photo voltage of the II–III cells tandem. Electric contacts (indicated in **Figure 3** left by arrows) are made to the external layers and to the interface of the first and the second cell.

As in our two-junction device, the transparent conductive layer (or heavily doped one) can be introduced in the contact region, to improve the electrical quality of the contact. Right part of **Figure 3** gives a scheme of construction of the three-junction solar cell device of our type. Here, 1 is the top active cell (i.e., $(p-i-n)_1$), 2 is the second one ($(n-i-p)_2$) and 3—the third ($(n-i-p)_3$), 4 is the interface contact (to the “ n ” regions of the cells 1 and 2, charged negatively under illumination), and 5—the two external contacts (to the “ p ” region of the cells 1 and 3, charged positively under illumination). The two contacts 5 must be interconnected, thus the first cell and the tandem of the two other cells with approximately the same photo voltage are connected in parallel, approximately doubling the photo current.

As in the previous case, we can reverse the layer’s sequence, just changing the sign of the voltage generated. Thus, the device of the type $(n-i-p)_1-(p-i-n)_2-(p-i-n)_3$ is equivalent to the one just described. Having only one tunnel junction instead of 2, our device is capable to have higher conversion efficiency than the traditional one.

For the four-junction solar cell device, we present the equilibrium energy band diagram in **Figure 4** (here, the four cells are denoted by numbers I, II, III and IV from left to right), and the construction scheme in **Figure 5** (left). The device has two insulating layers (4 and 7 in **Figure 5**); the part between them is a traditional two-junction tandem with one tunnel junction ($(n-i-p)_2-(n-i-p)_3$) whereas the two parts with an inside insulating layer comprise the two-junction converter of our design, the top one (with the larger band gaps) having the following sequence of layers: $(p-i-n)_1$ —insulating layer— $(n-i-p)_2$, and another one has the reversed sequence: $(n-i-p)_3$ —insulating layer— $(p-i-n)_4$. In **Figure 5** left, the number 3 corresponds to the top active cell I of the type $(p-i-n)_1$, number 5 shows the cell II with layer sequence $(n-i-p)_2$, 6 is cell III and 10 corresponds to cell IV. The contacts are made to the external layers of the device (1 and 12 in **Figure 5**, shown by arrows in **Figure 4**) and to the semiconductor layers adjacent to the insulating layers (another arrows in **Figure 4**, the two pairs 2 and 8, 9 and 11 in **Figure 5** left). As in the previous two cases, the transparent conductive layer (or heavily doped one) can be introduced in the contact regions, to improve the electrical quality of the contacts.

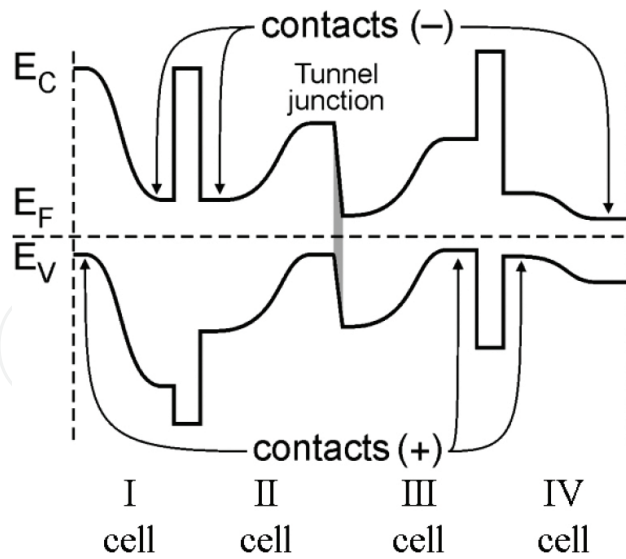


Figure 4. Energy band diagram of a four-junction device.

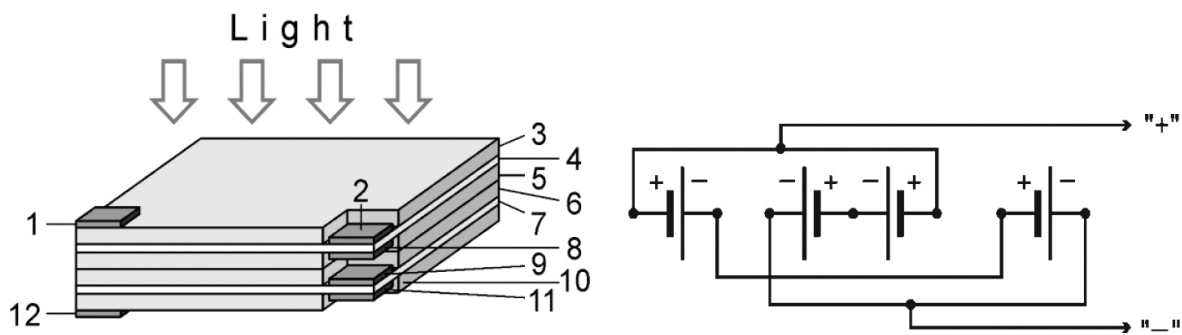


Figure 5. Construction scheme (left) and electrical connections (right) for a four-junction device.

Under illumination, the contacts to “ p ” layers are charged positively (1, 9 and 11 in Figure 5) whereas the contacts to “ n ” layers are negatively charged (2, 8 and 12 in Figure 5).

The photo voltage gradually decreases from cells I to IV; thus, it is natural to connect in series the top and the bottom cells (i.e., the cells I and IV) which gives approximately the same voltage as the tandem of the cells II and III; these two pairs (I–IV and II–III) must be connected in parallel. This cell connection is shown in Figure 5 right. Here, the contacts 2 and 11 of Figure 5 left are interconnected to provide the connection in series of the cells I and IV; the contacts 1 and 9 are connected making the “+” general output contact of the device, and the contacts 8 and 12 are connected making the “-” general output contact.

The cells’ materials must be chosen in such a way that the cells II and III comprising a traditional tandem device absorb equal amount of photons of the solar spectrum and produce the same photocurrent; the cells I and IV are also connected in series, so they have to absorb equal amount of photons and give the equal photo current, but this photon amount (and the photo current) is not necessarily equal to the amount of photons absorbed by the cells II and III and

their photo current. Thus in the present design, we have additional degree of freedom in division of solar spectrum among the active cells and more options for the efficiency optimization.

Again, the sequence of layers can be reversed without any principal changes (i.e., each of the semiconductor “*p*” layers might be substituted for the “*n*” layer, and vice versa). In relation to the antireflection coating, there is no difference from the traditional multi-junction device; again, the insulating layers with high refractive index must be recommended. Having only one tunnel junction instead of 3, our device is capable of having higher conversion efficiency than the traditional four-junction tandem solar energy converter.

2.2. Auto-concentrating multi-junction solar system

All the constructions above are assumed to be the monolithic devices similar in this sense to the traditional tandems; on the other hand, they can work either under normal or concentrated solar radiation, again as the traditional ones. Physical separation of the entrance solar cell (the one with *p-i-n* junction made of semiconductor material with the largest band gap) analyzed in this section presents additional degrees of freedom in total system’s design and some new possibilities of application.

The following construction is anticipated. The converter includes several entrance cells that are working in non-concentrated sunlight (cells I in **Figure 6**) and form the concentrating reflector for the part of solar spectrum that is not absorbed in these entrance cells, i.e., composed of photons with energies below the value of their band gap. For that, each entrance cell is designed in such a way that it specularly reflects the part of solar radiation with the photon energies below its band gap that is not absorbed by the cell. In the focal plane of this concentrator, the two-junction tandem converter is positioned (II and III in **Figure 6**). As illustrated in **Figure 7**, the cell I with the largest band gap possesses the interference antireflection coating 2 adjusted to minimize reflection of the solar radiation (1) with photon energies above the band gap, i.e., in the cell’s working spectral region, which is approximately 2–3 eV. The mean value

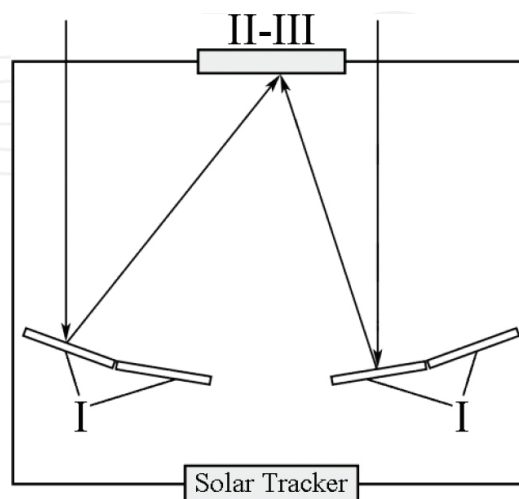


Figure 6. Auto-concentrating device.

for the wavelength in this region is $\lambda_1 \approx 500$ nm; from the condition of destructive interference of the light beams reflected from the two sides of the coating, we get the optimal thickness $d = \lambda_1/4N$ (N —refractive index of the coating material).

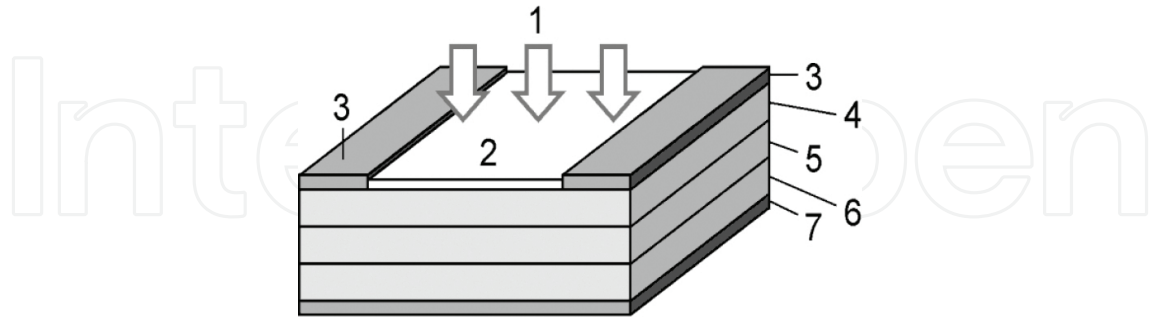


Figure 7. Construction of entrance cell I.

The other parts of the cell I are as follows: the top contacts 3, the semiconductor “ p ” layer 4, “ i ” layer 5, the “ n ” layer 6 and the back electrode 7. As in the previous cases, the sequence of layers can be reversed. The transparent conductive layer can be added at the top of the layer 4, to improve the contact electrical quality. The metal back electrode 7 has a mirror finish and, except for being a contact, serves as a mirror giving a specular reflection of the light passing the cell without absorption. This refers to the light with the photon energies smaller than the band gap E_{gI} (which is around 2 eV).

In relation to the photons with energies larger than E_{gI} , which are absorbed producing the photo voltage, cell I can be made with the active layers thickness half of that used in the traditional cell design, because in our cell, the light passes the active region twice. Except for the thickness reduction, this effect gives the more uniform photo excitation of the cell.

In the working region of the cells II and III (the mean photon energy is around 1.2 eV, the corresponding $\lambda_2 \approx 1000$ nm), the antireflection coating 2 of a cell I acts like a mirror: Here, the conditions for the constructive interference are held, $d = \lambda_2/2n$. This together with the mirror back electrode creates favorable condition for the specular reflection from the cell I of the major part of solar radiation not absorbed within the cell I. The reflected radiation is directed to the two-junction (cells II–III) device which scheme is not different from that shown in **Figure 1**.

Now, we add some details to the general scheme of the device discussed that is shown in **Figure 6**. Several cells I form concentrating reflector having the two-junction device with cells II–III in its focal plane. The area of each cell I is equal to the area of the two-junction device, and each cell I reflects its part of the incident solar radiation flux onto the II–III device; thus, the amount of light reflected by each cell I and falling onto the II–III device is multiplied by the number of these cells. All the cells of the device form a rigid construction; it is kept oriented to the Sun by the two-axis Sun tracking system (see [11, 12]).

The working region of the tandem II–III in the scheme of **Figure 6** corresponds to infra red radiation; some kind of heat engine can be used instead of this tandem (thermoelectric

generator TEG, Stirling engine, etc.) that will convert a device into an efficient hybrid solar system. Several examples of this construction were analyzed in papers [13, 14].

2.3. Summary

We have demonstrated that our original approach in construction of multi-junction solar energy converters allows wider choice of semiconductor materials and techniques of their production in comparison with the traditional design. As an immediate consequence, more economic converters can be developed and built. Our attempts of experimental realization of the possibilities thus arising are the subject of the following sections.

3. Technologies to realize all advantages of the new architecture

The total production cost of any device is determined by the cost of materials used and of the technology employed. We have already mentioned that the possibility of utilization of semiconductor materials of the groups II–VI, IV and IV–VI greatly widens the choice of economic and abundant raw materials for the energy converting devices. On the other hand, the corresponding technologies must be also economic, easily scalable, consuming small amount of energy and ecologically friendly: Devices for production of clean energy demand clean technologies. Below, we briefly describe the available technologies of this kind, in particular, their versions that we have employed and developed.

3.1. Eco-friendly chemical and photo chemical bath deposition; SILAR

Chemical bath deposition is a well-known and used more than 100 years technique (see review [15]), previously for production of photo detectors such as PbS and PbSe, and more recently, in thin film solar cells. Nowadays, it became much more popular because with it the nanocrystalline or nanoporous materials can be grown. It is easily scalable, low temperature and little energy consuming. It is not necessarily ecologically pure. For example, chemically deposited CdS window layers have been used in the last years in high efficiency CdTe/CdS and CIGS/CdS solar cells. However, the chemical deposition of CdS thin films by generally accepted CBD recipes at large scale could raise serious environmental problems because this process usually utilizes ammonia which is highly volatile, toxic and thus harmful to the environment. Furthermore, the volatility of ammonia changes the pH of reaction solution along the deposition process and hence results in irreproducible film properties [16]. Thus, the search for new chemical deposition processes to obtain chalcogenide semiconductor films with applications in large scale, which involve some solutions to the environmental issues, is now of great practical interest.

In the last few years, in our group, we have developed convenient alternative CBD processes for the growth of good quality CdS and CdSe thin films (see, for example, [16, 17]). We found that ammonia-free chemically deposited CdS layers perform quite well as window layers in CdTe/CdS solar cells and as semiconductor active layers in thin film transistors [18, 19]. Below, we give some examples of application of CBD and its derivatives (PCBD and SILAR) for

production of material such as CdS, CdSe, CdTe, PbS, PbSe, PbTe and some devices based on them. In particular, we developed CdS/PbS solar cell with energetic efficiency of 1.6% and quantum efficiency of 25% (**Figures 8 and 9**) using only ammonia-free CBD process [20].

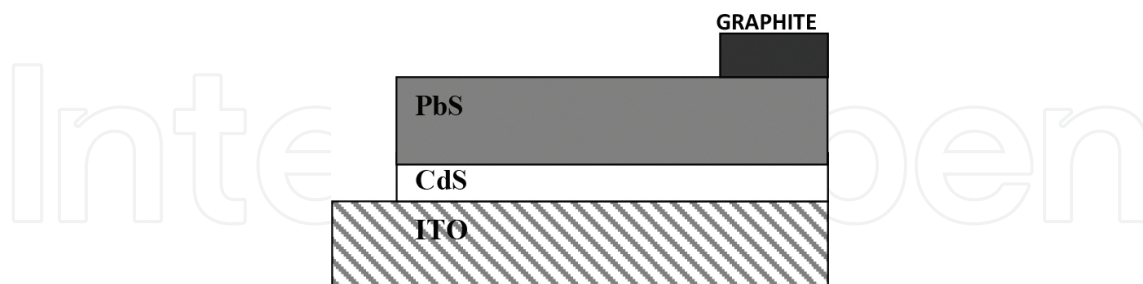


Figure 8. Construction of CBD CdS/PbS cell.

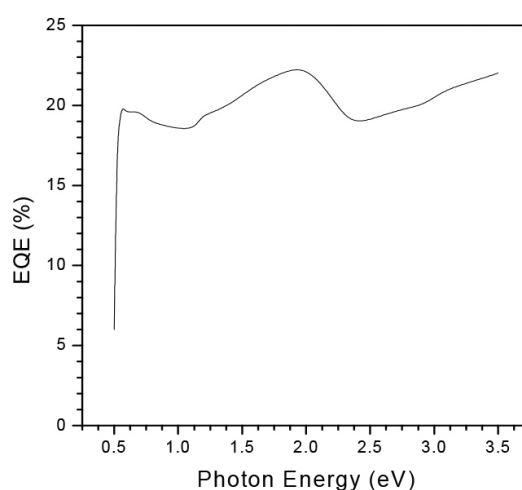


Figure 9. Cell's quantum efficiency.

The photo chemical bath deposition (PCBD) process basically repeats a traditional CBD, with addition of UV illumination. There are two types of UV lamps: the short wave ones (265 nm) and the long wave (365 nm); both were used. The UV illumination of the solution has a purpose to promote the reaction, which can be realized without this radiation, but will take much more time. For example, in the specific case of deposition of plumbonacrite $6(\text{PbCO})_3 \cdot 3(\text{Pb}(\text{OH})_2) \cdot \text{PbO}$ that can be later used for production of PbS, PbTe, etc., the reaction duration with UV radiation shortens approximately 20 times.

The deposition process was carried out at room temperature (25°C) in a flat beaker with a total area of 20 cm²; the deposition area is just limited by the size of the beaker and the irradiated area, so this process can be reproduced in large scale. The plumbonacrite film was deposited in a solution prepared in a flat beaker by the sequential addition of 20 ml at 0.2 M of $(\text{CH}_3\text{COO})_2\text{Pb} \cdot 3\text{H}_2\text{O}$, (lead acetate, trihydrate), 20 ml at 0.4 M of $\text{C}_6\text{H}_5\text{Na}_3\text{O}_7 \cdot 2\text{H}_2\text{O}$ (sodium citrate, dihydrate), at this point, the solution presents a white color; then, it should be quickly

added with 20 ml at 0.5 M of KOH (potassium hydroxide) and deionized water to fill a total volume of 80 ml. Then, the solution was placed under UV radiation with a UV lamp (365-nm-long wave radiation, 22 W, see **Figure 10**) at room temperature to realize a PCBD process; a white dense thin film appears after 5 h. Without illumination, the deposition time necessary is almost 20 times larger. The dissociation of lead acetate gives the metal ions with the action of the complexing agent, also provides the basis for the formation of CO_3^{2-} ions, as well as the KOH provides OH^- , O^{2-} and K^- ions, which are employed in the main reaction.

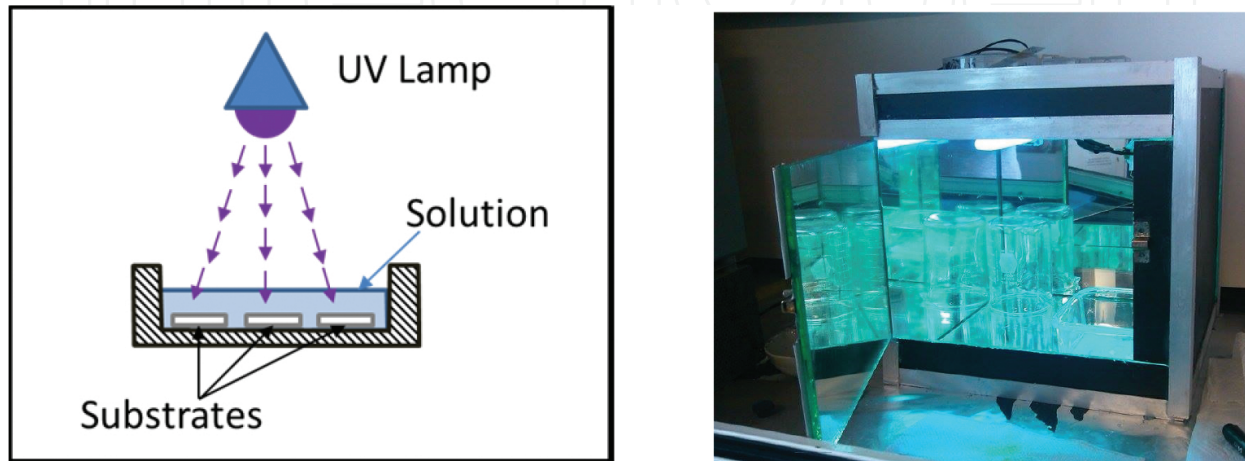


Figure 10. Photo chemical bath deposition scheme and photo of the actual bath.

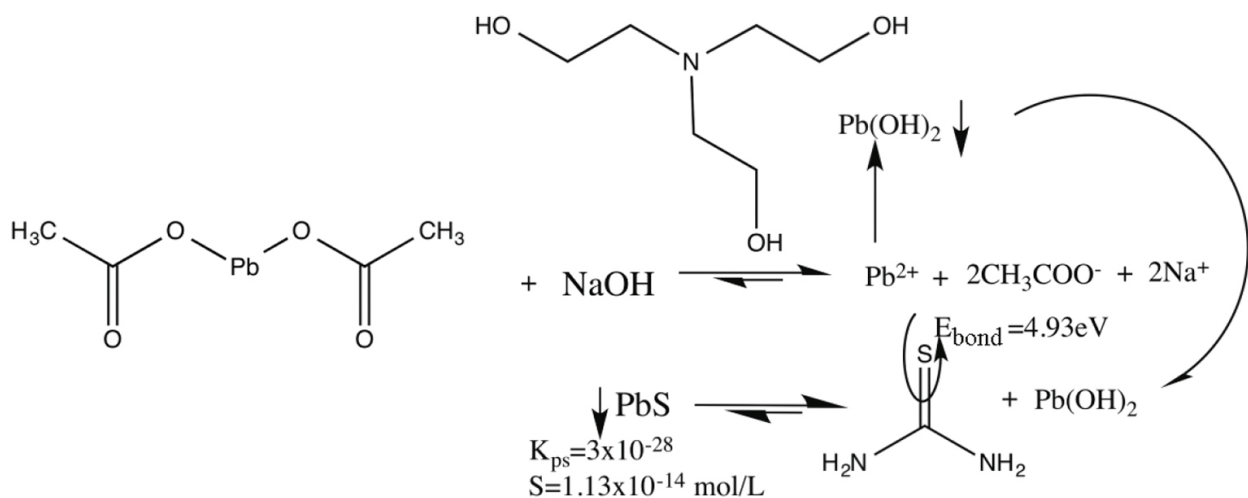


Figure 11. Simple cluster reaction mechanism.

The next example to illustrate the action of UV illumination in the CBD processes is the particular case of deposition of PbS film. The standard CBD reaction involves two steps, nucleation and particle growth. The film growth can take place either by ion-by-ion condensation of materials or by adsorption of colloidal particles from the solution on the substrate [21, 22].

The PCBD reactions, for this study, follow the same pathway that the CBD one, where the UV lamp provides energy to the reaction (see explanation below). The CBD reaction involves two reactions mechanism, the first one consists of simple cluster (hydroxide) mechanism, which occurs when the formation of the lead hydroxide takes place. Pb^{2+} ion results from $Pb(OH)_2$ at basic pH in aqueous solution; Trietanolamine (TEA) inhibits the precipitation of $Pb(OH)_2$ and allows the hydroxide to break the double bond $C=S$ of thiourea yielding S^{2-} ion. Coupling of Pb^{2+} and S^{2-} ions renders PbS . The energy required to break $C=S$ bond is 4.93 eV, this energy corresponds to photon within the UV region. When the PbS exceeds the solubility constant (K_s), the PbS starts to precipitate, see **Figure 11**.

The second reaction mechanism, ion-by-ion mechanism, involves the hydrolysis of the thiourea [23]. This reaction mechanism generally occurs at acid pH, but the amphoteric behavior of water triggers the spontaneous hydrolysis of thiourea. For this reaction to occur, it is also necessary to break the bond between atoms C and S (see **Figure 12**).

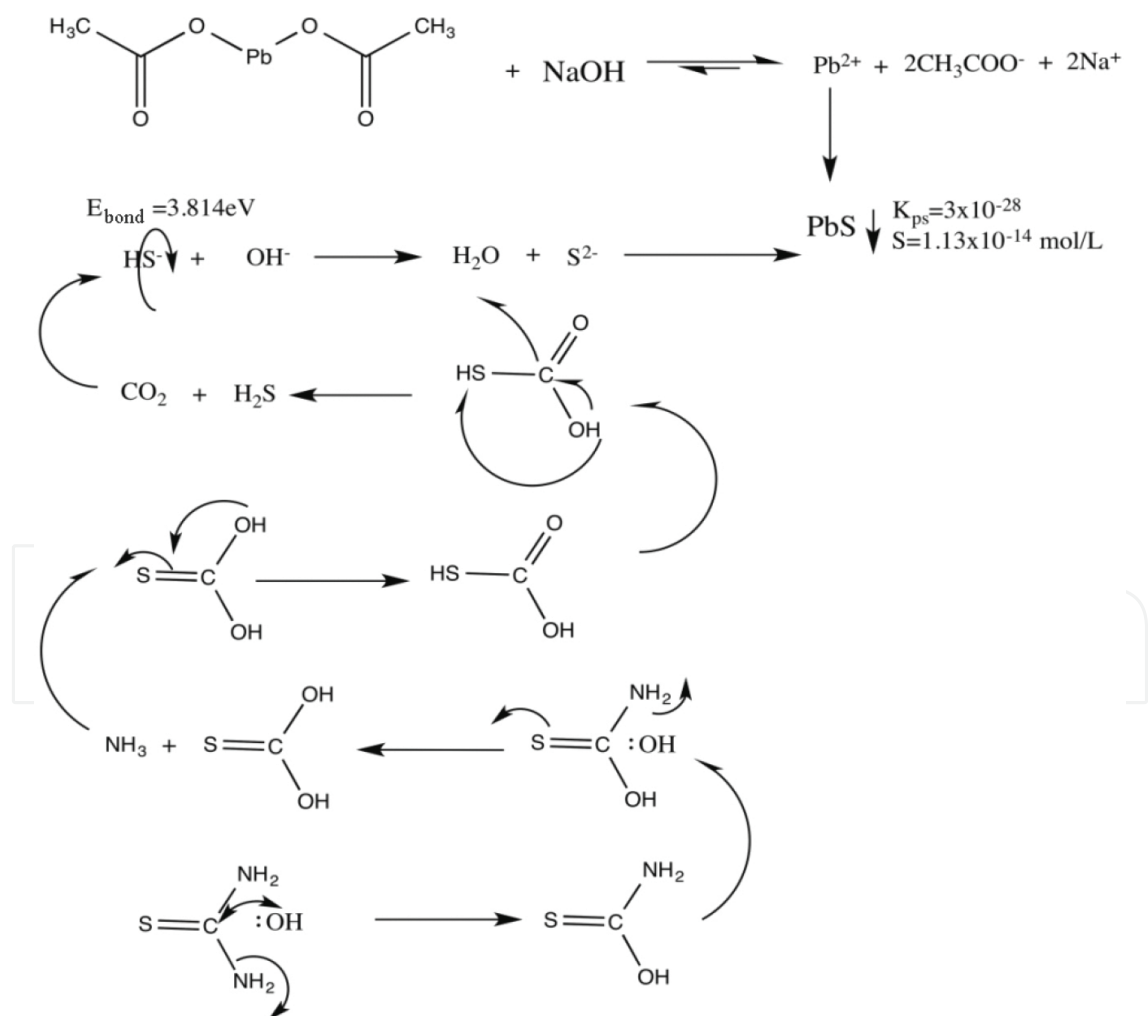


Figure 12. Ion-by-ion reaction mechanism.

It refers to the hydrolysis of the thiourea. The energy needed to break this bond is 3.81 eV. As in the simple cluster mechanism, the energy necessary to cleave bonds involved in the reaction is within the UV spectral region; in this way, UV lamp provides energy to the reaction thus further promoting the formation of the PbS.

3.1.1. Successive ionic layer adsorption and reaction technique (SILAR)

The SILAR method involves the immersion of the substrate separately into solutions, alternating cationic and anionic ones; besides, a process can involve an inter step between the cationic and anionic treatment, which usually is an immersion of the substrate into deionized water in order to remove a solution excess or badly adsorbed particles. For example, we describe how with SILAR, we obtained cadmium oxide hydroxide that by annealing can be easily converted to transparent conductive oxide (TCO) CdO for application in solar cells [24].

The process includes four following steps (highlighted with numbers in **Figure 13**): (1) immersing the substrate in the cadmium-rich solution for 20 s to create a thin liquid film containing a complex that includes cadmium ions onto the substrate; (2) immediately immersing the withdrawn substrates in hydrogen peroxide solution for 20 s to form a $\text{Cd}(\text{O}_2)_{0.88}(\text{OH})_{0.24}$ layer; (3) drying the substrate in air for 60 s; and (4) rinsing the substrate in a separate beaker for 20 s to remove loosely bonded particles. Only three cycles are necessary to form a white transparent layer of $\text{Cd}(\text{O}_2)_{0.88}(\text{OH})_{0.24}$ over the substrate. The thickness of the film is controlled by the number of cycles, thus for a thicker layer, several cycles are needed. Up to 50 cycles was done in order to study the kinetics of growth.

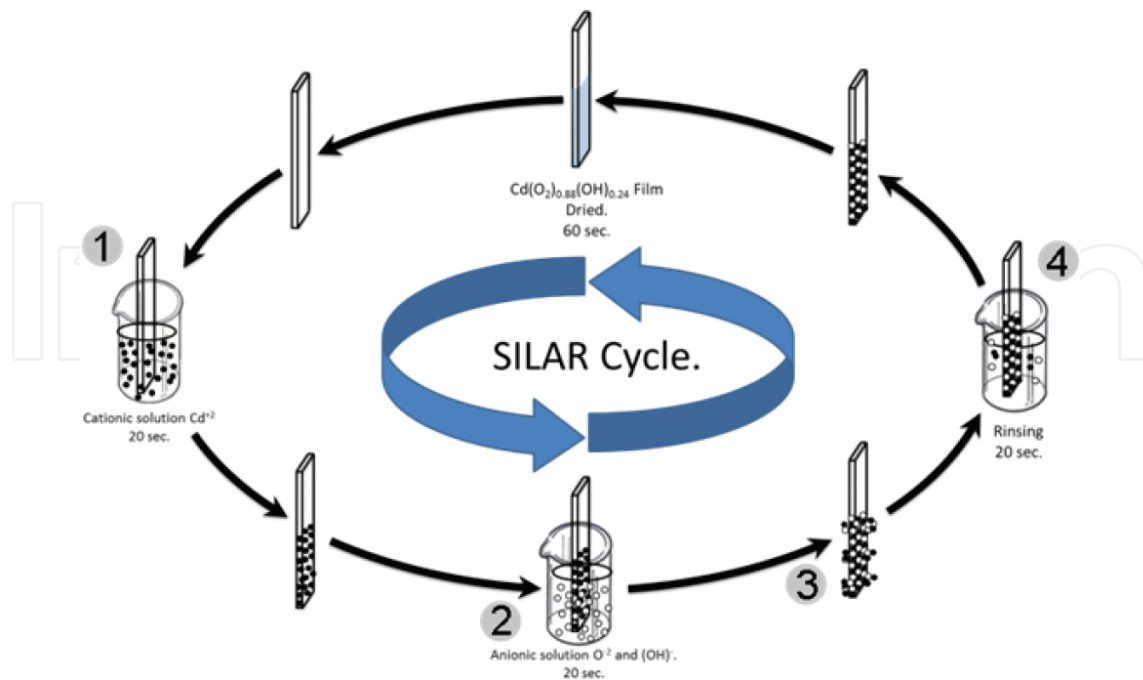


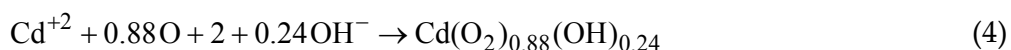
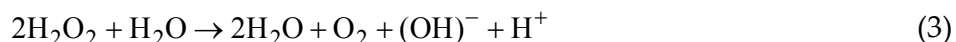
Figure 13. SILAR cycle.

An important issue for the development of semiconductor films is the thickness control. In this regard, SILAR-CBD is a technique that offers an effective and easy way to control the film thickness by a number of cycles. In particular, for this specific process, each cycle adds 21 nm of thickness.

The mechanism of $\text{Cd}(\text{O}_2)_{0.88}(\text{OH})_{0.24}$ film formation by SILAR method can be illustrated as follows. We used two main solutions; the first one with cadmium ions is composed of cadmium acetate $\text{Cd}(\text{CH}_3\text{CO}_2)_2$ (0.1 M) as a source of Cd^{2+} ions. In order to produce a complexed Cd^{2+} ion, we add triethanolamine $\text{C}_6\text{H}_{15}\text{NO}_3$ (0.5M) as complexing agent ($\text{pH} = 9$ of solution). Eq.(2) below describes the chemical reactions.



When the substrate is immersed in the above solution, these complexed cadmium ions are adsorbed onto the substrate due to attractive force between ions in the solution and surface of the substrate. These forces can be Van der Waals forces, cohesive forces or chemical attractive forces. The substrate is then immersed in dilute H_2O_2 solution to convert the cadmium complex into $\text{Cd}(\text{O}_2)_{0.88}(\text{OH})_{0.24}$ by the following reactions



3.2. Chemical vapor deposition with several evaporation sources

For CVD process, we have built Hot Wall CVD reactor with three sources of hot atomic gas transported to substrate with a neutral gas flow (nitrogen or argon). The scheme of the reactor is presented in **Figure 14** (here, we show only one Te source).

The actual reactor is a quartz cylinder (**Figure 15**) with the length of 120 mm and internal diameter of 74 mm, opened at the top and having four quartz tubes at the bottom with diameter of 12 mm and length of 335 mm. The tubes serve for transport gas input and exit and for positioning of the sources for material evaporation.

Thus, three sources could be used simultaneously, with separate regulation of gas flux for each of them, and with the possibility of using two or three different gases in the same experiment. The maximum dimensions of the films deposited are restricted by the cylinder's internal diameter. The substrate holder for material deposition is placed at the top of reactor. It consists of graphite ring with graphite plate having four windows of $10 \times 10 \text{ mm}^2$ each that define dimensions of actual samples, and the upper vacuum-tight cover that prevents a gas escape from reactor.

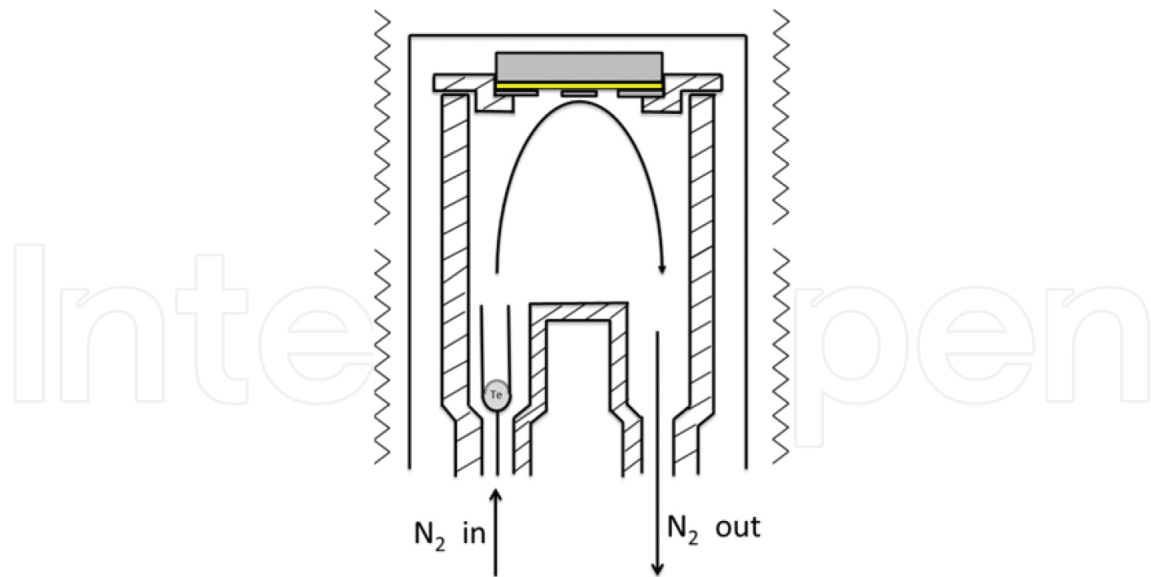


Figure 14. General scheme of CVD hot wall reactor.



Figure 15. Upper part of quartz reactor with sample holder and substrate.

The reactor is fixed on the metallic base (**Figure 16**) that contains the elements necessary for gas input, output and flow control as well as for measurements of the material source's temperatures; besides, it has double walls with water circulating between them, to keep the ambient temperature of the gas leaving the reactor through the water seal thus avoiding a possible leakage of toxic gases. The active part of the reactor containing sources and substrate is placed within an oven that is divided in two parts having separate regulation of electric current passing through their heating resistances, so that necessary temperatures of sources and of substrate can be chosen and maintained. According to the accepted classification, this reactor is a hot wall reactor which is surrounded by heating system that can reach a maximum temperature of 900°C in substrate and source part separately. A special computerized system was designed and made for programming and automatic monitoring of all stages of the deposition process. When two atomic sources were used (for example, to deposit CdTe or CdSe

films), they were placed within Knudsen cells, and the evaporation rate was controlled by the cells opening diameters, and their temperature. The transporting gas flux was chosen to provide laminar flow in all parts of the reactor; the character of the flow was studied by simulation, using program COMSOL Multiphysics 4.4.

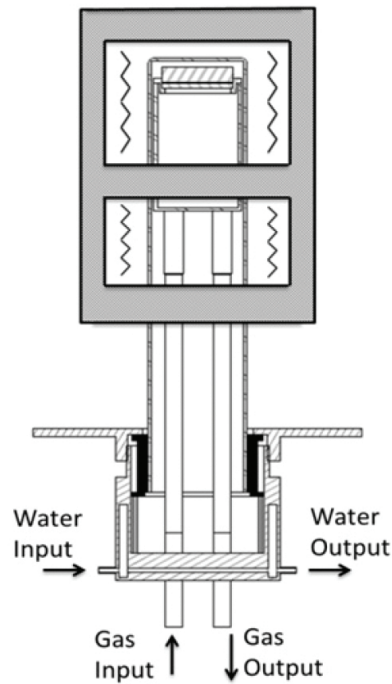


Figure 16. Quartz reactor fixed to the base.

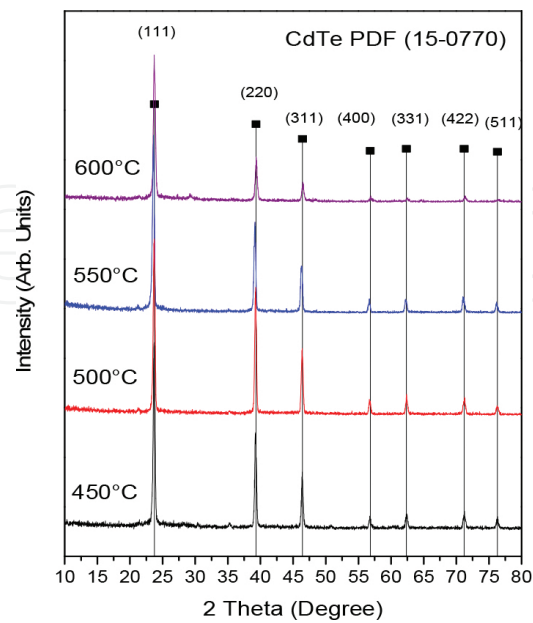


Figure 17. X-ray analysis of CdTe samples (see text).

Figure 17 presents X-ray diffraction pattern obtained on CdTe film deposited in our reactor at different temperature of both sources of Cd and Te (the temperature is given by the reactor's Hot Walls). The character of the pattern showed a polycrystalline nature for all films, which is consistent with the standard cubical structure of cadmium telluride (PDF 17-0750; the significant peaks observed at $2\theta = 22.73^\circ, 39.31^\circ, 46.44^\circ, 56.83^\circ, 62.45^\circ, 71.11^\circ$ and 76.25° are indexed as (111), (220), (311), (400), (422) and (511), respectively).

3.3. Two-stage CBD/CVD technique

We also developed the two-stage process for deposition of II–VI and IV–VI semiconductor films, namely CdTe, CdSe, PbS, PbSe and PbTe. Here, we illustrate this two-stage process with an example of obtaining of PbTe films from precursor plumbonacrite deposited by some variety of chemical bath deposition. In the first stage, plumbonacrite $\text{Pb}_{10}(\text{CO}_3)_6\text{O}(\text{OH})_6$ was deposited onto glass substrate by PCBD, using ammonia-free low-temperature process in alkaline aqueous solution. Then, in the second stage, the obtained film was placed in our CVD reactor described in the previous section, where it acted as substrate in a reaction of substitution of nonmetallic film component by Te, thus forming PbTe films. The nitrogen flux of 0.25 lt/min was used as transporting gas. The source temperature was adjusted between boiling (T_b) point and melting point (T_m) with the aim to control the flux gas of the source (Te source, $T_m = 449.51^\circ\text{C}$, $T_b = 988^\circ\text{C}$). The substrate temperature was adjusted to improve the quality of the film (see [25, 26] for details).

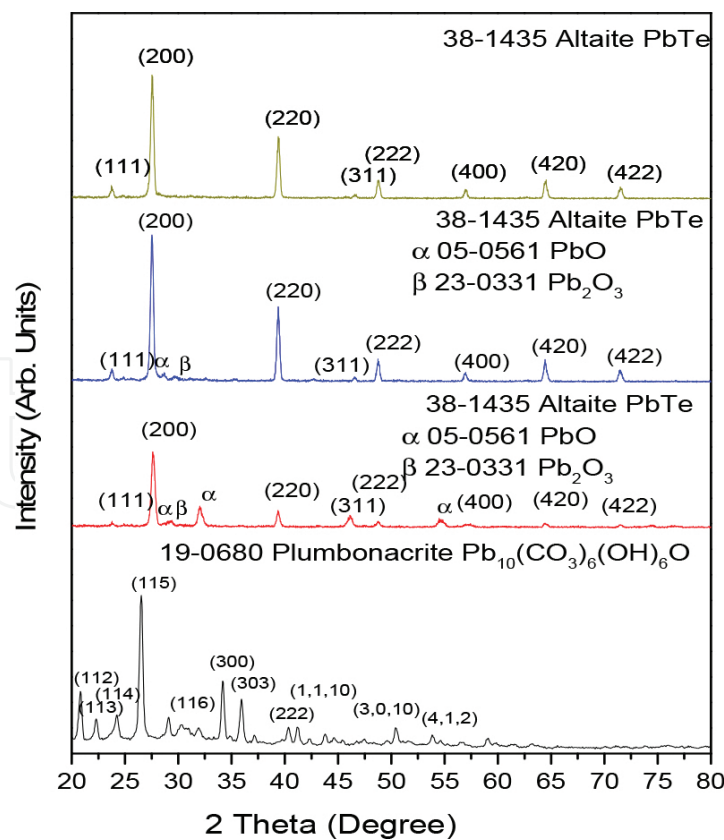


Figure 18. Illustration of development of PbTe in CVD reactor.

XRD patterns for plumbonacrite film and the film after tellurium gas treatment are shown in **Figure 18**. The character of the pattern and the peaks intensities show polycrystalline nature for all films. At the bottom of **Figure 18**, it is possible to see the plumbonacrite diffraction pattern which is consistent with the standard hexagonal structure of plumbonacrite (powder diffraction file 19-0680), and after telluride gas treatment (20, 40 and 60 min), the plumbonacrite structure suffers a change turning from hexagonal structure to cubical structure of lead telluride. The total conversion to lead telluride from plumbonacrite takes place at 60 min; the conversion time depends on the film thickness. For 20 and 40 min of treatment, it is possible to appreciate that the plumbonacrite film starts to decompose into lead oxides as PbO (PDF 05-0561) and PbO₂ (PDF 23-0331), and later these also turn into lead telluride. This fact is possible to confirm by observation that peaks appearing at 20 min decrease at 40 min and vanish at 60 min, where only the planes associated with the lead telluride (PDF 38-1435) remain.

In a similar manner, we obtained CdTe and CdSe films using as a substrate in CVD reactor, the cadmium oxide hydroxide Cd(O₂)_{0.88}(OH)_{0.24} film produced by some of the CBD versions; the sources of Te and Se were used in a CVD process, correspondingly for CdTe and CdSe. Using Si as a substrate in the first (CBD) stage, we get rectifying structures as *n*-Si/*p*-PbTe acting as photodiode or a component of multi-junction solar cell.

The SEM images (**Figure 19**) show that the material precursor is composed of small spherical grains with an approximate size of 500 nm; after CVD, the resultant CdSe film has a grain size of 2–3 μm. The composition of the precursor film was studied with EDAX complement to SEM, and it has shown the composition of the CdSe film with a Se/Cd ratio of 0.915. The lateral micrograph gives an estimate for the film thickness: The precursor film has a thickness of 15 μm, and the CdSe film has the same thickness after 30 min of CVD. The investigated optical and structural properties of the films obtained do not differ from those of the bulk material, evidencing the good quality of the material made.

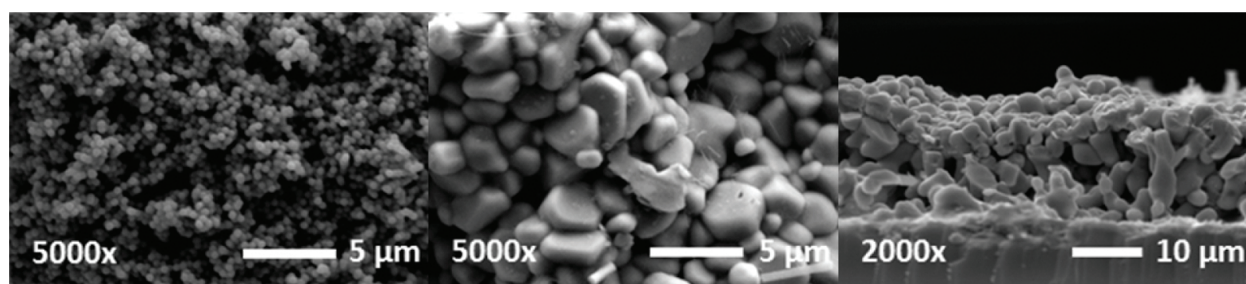


Figure 19. Left to right: frontal image of precursor film, frontal and lateral views of CdSe film.

3.4. Summary

We see that the techniques described can be successfully used for production of the multilayered (multi-junction) devices for solar energy conversion, providing simple, easily scalable, economic and ecologically friendly processes.

4. First results: multilayered photo diodes and solar energy converters based on II–VI and IV–VI semiconductor materials

In the sections above, we described a variety of semiconductor materials obtained with ecologically friendly and simple techniques. Application of these materials for design and construction of economic photo sensitive structures and solar energy converters is a great project in which we are engaged now. We already mentioned a solar cell based on CdS/PbS films developed by pure chemical route [20]. Below, we give two examples of the two-layered devices already developed—a light sensing photo diode based on Si/PbTe, and a CdS/CdTe-based solar cell.

4.1. Structure and parameters of *n*-Si/*p*-PbTe photo diode

The deposition of the main components of the device was described above (that of plumbonacrite on Si substrate by PCBD in 3.1, its transformation to PbTe in 3.3). Hall measurements show *p*-type conductivity of PbTe, the results are presented in **Figure 20**.

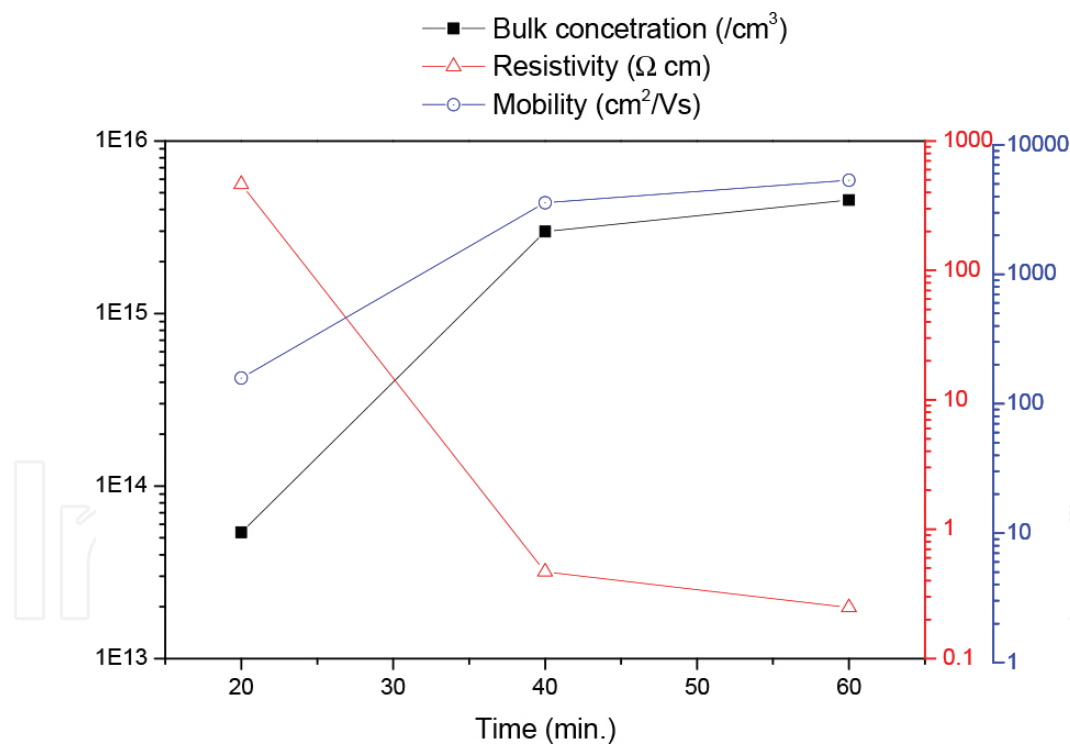


Figure 20. Electrical parameters of PbTe film.

Hole concentration in PbTe was increasing with an increase in the treatment time under tellurium hot gas up to $10^{16}/\text{cm}^3$, with mobility changes from 150 to $700 \text{ cm}^2/\text{V s}$. The **Figure 21** gives the device structure (insert) and the I–V characteristics under illumination with tungsten lamp providing a total irradiation of $1500 \text{ W}/\text{m}^2$.

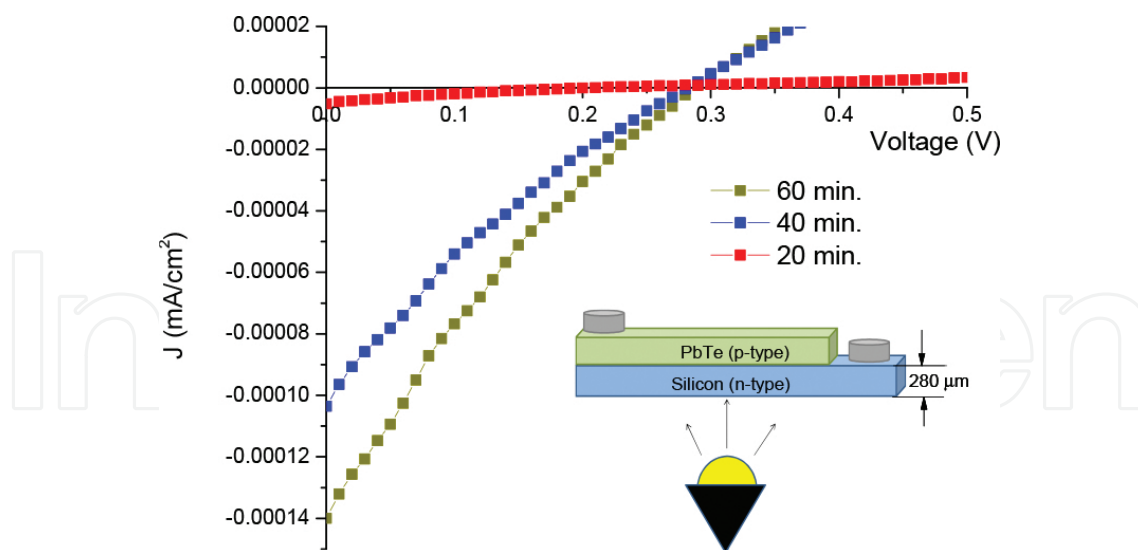


Figure 21. Current-voltage characteristics of a diode depending on Te gas treatment.

The device was illuminated from the silicon side which has a thickness of 280 μm . The characteristics observed are typical of a solar cell, but with very poor fill factor and efficiency, so there is an open field for the cell optimization.

However, if the structure is treated as a light sensor (photodiode), its main parameter is the photo responsivity (photo current per watt of light intensity); in our case, it is $S = 0.1 \text{ A/W}$, quite comparable with responsivity of commercial photo diodes (for example, commercial GaP/Au photo diode has sensitivity $S = 0.15 \text{ A/W}$ [27]). Except for this photo diode, we elaborated two other bilayered photo diode structures: One with *n*-Si/*p*-CdTe active layers having the responsivity $S = 1.4 \text{ A/W}$, and another of *n*-CdS/*p*-PbS, with $S = 1.2 \text{ A/W}$. Thus, we demonstrate that our sensors photo diodes can be superior to some commercial ones.

4.2. Investigation of CdS/CdTe semiconductor structure for solar cell

The *n*-CdS/*p*-CdTe bilayered structure is a core of a special type of solar energy converters that are already in the market, with relatively large annual production (First Solar Company) and acceptable efficiency of around 14% [28, 29]. Our purpose was not the repetition of their construction scheme and techniques, but investigation of the properties of this active bilayered structure as a function of the deposition parameters which we can control using our technologies that are different from those employed in First Solar, with an idea that this (or similar) structure can serve as a part of our future multilayered converter. In particular, we investigated an effect of CdCl₂ treatment upon the structure parameters.

The 300-nm-thick CdS layer was prepared by CBD on glass substrate covered with a thin conducting layer of ITO (see [20]), and CdTe film was deposited over this layer in our CVD reactor with two atomic sources. For these sources, we employed Knudsen cell with Cd having an opening of $1.96 \times 10^{-6} \text{ m}^2$, and for Te – $3.17 \times 10^{-5} \text{ m}^2$ that gives approximately equal atomic flux of both components in the deposition region. A special attention was given to the uniformity of CdTe film thus obtained: The results of the simulation of the gas flow in the reactor

were used to adjust the deposition parameters (the temperatures and the neutral gas flow). As seen in **Figure 17** above (Section 3.2), CdTe polycrystalline films with standard cubical structure were obtained at sources temperatures from 450 to 600°C (the substrate temperature at all cases was kept smaller by 50°C); average crystal size found from the diffraction peak width was around 30 nm, growing slightly as the temperature increases.

Figure 22 shows that deposition temperature had a marked effect on the grain size: It increases as the temperature increases, being 0.37 μm at 450, 1.67 μm at 500, 3.02 μm at 550 and 6.4 μm at 600°C. It is well-known that large grains are favorable for solar cell's materials. Optical data agree with X-ray diffraction giving 1.5 eV band gap that is normal for cubic crystals (see **Figure 23**, inset show position of the derivative of absorption coefficient with sharp peak at 1.5 eV).

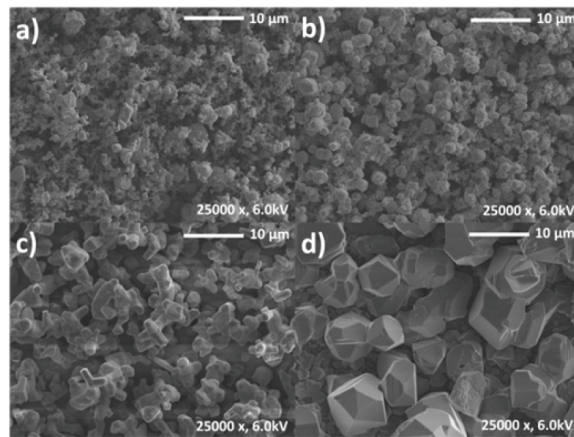


Figure 22. SEM images of CdTe films at different sources temperature: 450°C (a), 500°C (b), 550°C (c) and 600°C (d).

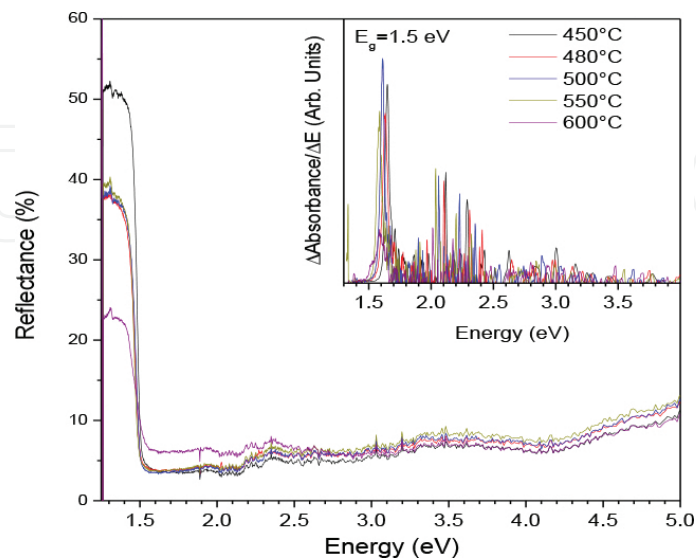


Figure 23. Reflection spectrum of CdTe film and its derivative (insert).

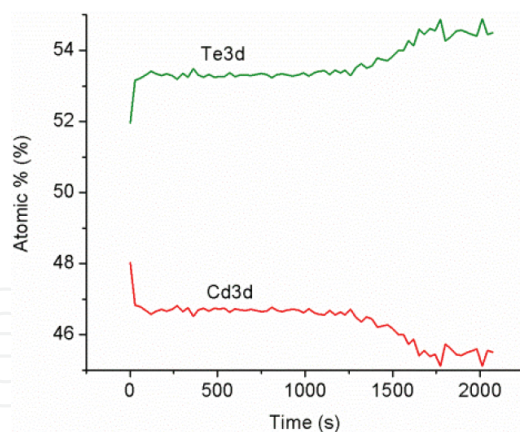


Figure 24. Atomic distribution in CdTe (see text). External boundary at the left.

XPS data (**Figure 24**) give the atomic distribution along the CdTe film. The abscissa shows the etching time (2000 s with etching rate of 0.66 nm/s gives the film thickness of 1.32 μm , etching rate was calibrated with Ta_2O_5 standard). We see a considerable excess of Te, especially in the internal part of the film (right edge, **Figure 24**).

The variation of the Te 3d signal binding energies (**Figure 25** for Te 3d level; for Cd, we have similar data) shows the oxidation effects (the presence of oxygen) at near-surface region, significant at about two thirds of the film's thickness.

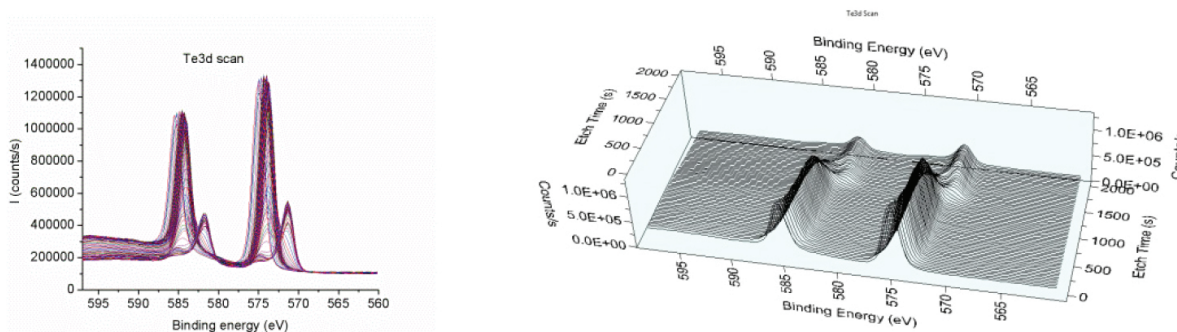


Figure 25. XPS binding energies for Te 3d level in CdTe (see text).

Binding energies for the Te 3d signal of the Te $3d^{5/2}$ 575 eV and Te $3d^{3/2}$ 585 eV at the outmost part of the cell, and shifting to Te $3d^{5/2}$ 572 eV and Te $3d^{3/2}$ —582 deeper in the cell. According to NIST database [30], internal values are those characteristic for the bulk CdTe, external are shifted to higher energies due to oxidation.

It is known that an excess of Te (vacancies of Cd) produces acceptors in CdTe, but the oxygen (isovalent impurity) acts as a donor [31], so the resulting conductivity is unclear. Measuring the sample work function with Kelvin Probe equipment, we came to the conclusion that CdTe film in our CdS/CdTe system is of *n*-type, see the band diagram (**Figure 26**, solid lines).

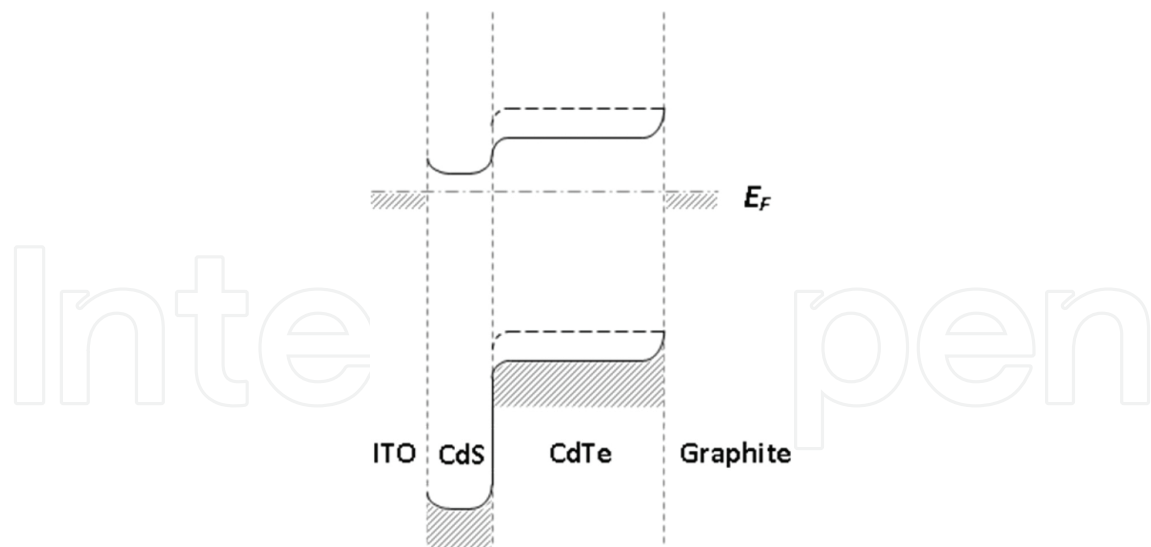


Figure 26. Band diagram of a CdS/CdTe structure.

In **Figure 26** we see, first of all, the barrier of around 0.25 eV between the c-bands of CdS and CdTe, and upper curving of both bands of CdTe at its surface near the graphite electrode by another 0.25 eV. Correspondingly, we observed photo voltage generation of approximately 0.25 V when illuminating the structure from each side.

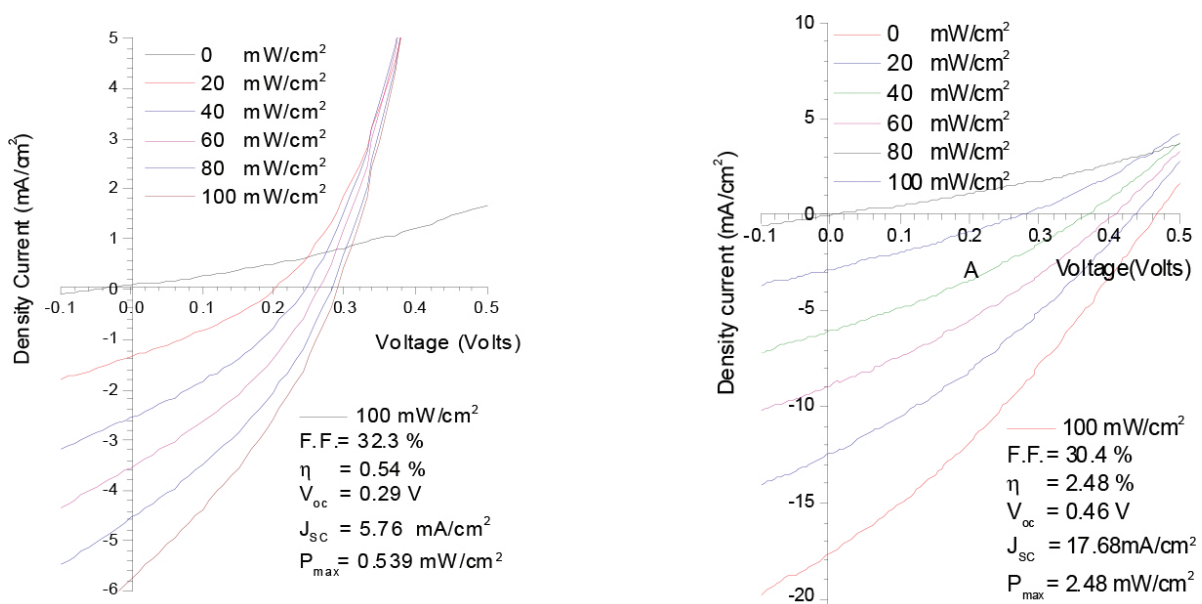


Figure 27. I-V curves of CdS/CdTe solar cell before (left) and after (right) the CdCl₂ treatment.

Slight upper band curving in CdS near contact with ITO is a consequence of higher work function of the ITO compared to CdS.

Solar cell based on this structure possesses modest characteristics (**Figure 27** left) with the efficiency of less than 1%, the open circuit voltage V_{oc} of 0.3 V and the short circuit current of

I_{sc} 6 mA/cm². A standard treatment with CdCl₂ (10 min in saturated solution, then rinsing and annealing at 300°C for 2 h) drastically changes all characteristics, as expected (**Figure 27** right, [32]): much larger values of I_{sc} , V_{oc} and efficiency. Since the mechanism of this treatment action is still not quite clear, we perform some study to find out just what parameters are affected by the treatment. It is already known that the treatment enhances grain growth. Our SEM images show that, indeed, after the treatment much larger grains appear.

Besides, these images show (**Figure 28**) that before the treatment (left image), the definite boundaries separating individual grains are observed, but after treatment (right image) the grain separation practically disappear, as if the grains were melted. The other factors that we found are an increase in the photoconductivity of the CdTe film (i.e., increase the lifetime of nonequilibrium charge carriers) and improvement of the stoichiometry: According to the EDAX data, the atomic ratio of Cd and Te was 0.953 before treatment, and became 0.977 after it. The CdTe film remained of *n*-type, but the barrier between the c-bands of CdS and CdTe increased to 0.5 eV as shown in **Figure 26** by the dashed lines, giving the corresponding increase in the cell's open circuit voltage. The fact that the Fermi level in CdTe lies above the middle of the band gap agrees with observation made in Ref. [33].

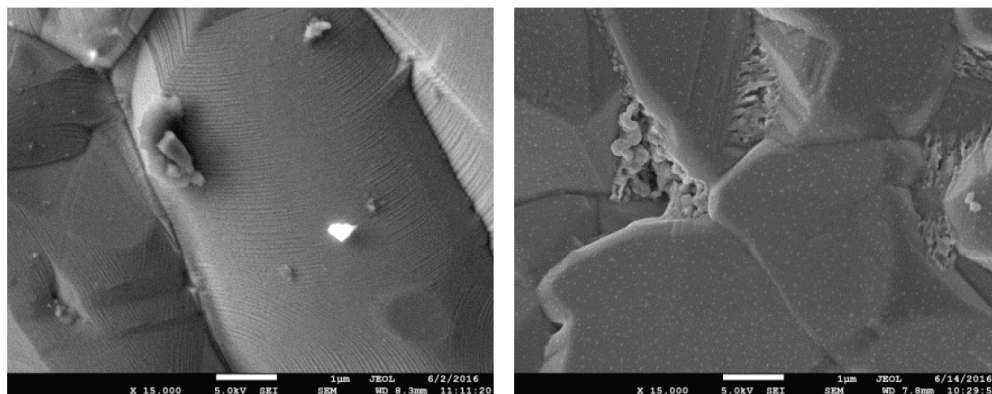


Figure 28. Effect of CdCl₂ treatment upon morphology of CdTe.

We see that the standard construction of CdS/CdTe cell made with standard treatment is not ideal for solar energy conversion, giving the incorrect conductivity type of the main absorber material, and having additional serial resistivity at the ITO/CdS contact. Therefore, we plan to study the different constructions with the different treatment for application in the multilayered solar energy converter.

4.3. Summary

It is shown that with technologies utilized, efficient photo sensors can be made based on semiconductors II–VI and IV–VI, with better parameters than devices present in the market made of III–V semiconductor GaP. It is also evident that these techniques have a great potential in development of efficient and economic solar energy converters.

5. Conclusions

We demonstrated that following our original approach in construction of multilayered semiconductor photovoltaic devices and using ecologically friendly and small energy consuming technologies, particularly the ammonia-free chemical routes and photo chemical bath deposition technique developed in our group, economic and efficient devices can be made. We believe that this is the way towards the economic and efficient solar energy converters for terrestrial applications.

Acknowledgements

I.R. Chávez-Urbiola wishes to thank CONACYT for his scholarship. Y.V. Vorobiev thanks CONACYT (project #259982) for financial support of his sabbatical leave to CIMAV Campus Monterrey. We acknowledge the technical assistance of Luis Gerardo Silva Vidaurri, C.A. Avila Herrera, J.E. Urbina Álvarez and A. Jiménez Nieto.

Author details

Yuri V. Vorobiev^{1*}, Iker R. Chávez Urbiola¹, Rafael Ramírez Bon¹, Liliana Licea Jiménez², Sergio A. Pérez García², Pavel Vorobiev² and Paul Horley²

*Address all correspondence to: vorobiev@cinvestav.mx

1 CINVESTAV-Querétaro, Libramiento Norponiente 2000, Querétaro, QRO, México

2 CIMAV/Monterrey, Parque de Investigación e Innovación Tecnológica, Apodaca, NL, México

References

- [1] H. Cotal, C. Fetzer, J. Boisvert *et al.*, III–V multijunction solar cells for concentrating photovoltaics, *Review Energy and Environmental Science*, vol. 2, pp. 174–192, 2009.
- [2] A. Hoffmann, U. W. Paetzold, C. Zhang *et al.*, Advancing tandem solar cells by spectrally selective multilayer intermediate reflectors, *Optics Express*, vol. 22, pp. 1270–1277, 2014.
- [3] O. Isabella, A. Hendrikus *et al.*, Thin-film silicon-based quadruple junction solar cells approaching 20% conversion efficiency, *Solar Energy Materials and Solar Cells*, vol. 129, pp. 82–89, 2014.

- [4] Y. Vorobiev, J. González-Hernández, H. Esparza-Ponce, and P. Gorley, Mexican Patent No. 274256, 2010.
- [5] Y. Vorobiev, J. González-Hernández, H. Esparza-Ponce, and P. Vorobiev, Mexican Patent No. 312841, 2013.
- [6] I. R. Chávez-Urbiola, Y. V. Vorobiev, and R. Ramírez Bon, New principles in design and technology of multi-junction solar energy converters, *International Journal of Materials, Mechanics and Manufacturing*, vol. 4, no. 1, pp. 80–84, 2016.
- [7] W. Shockley, and H. J. Queisser, Detailed Balance Limit of Efficiency of p - n Junction Solar Cells, *Journal of Applied Physics*, vol. 32, pp. 510–519, 1961.
- [8] Spectrolab website <http://www.spectrolab.com/solarcells.htm>
- [9] D. Kanama, and H. Kawamoto, Science and technology trends, *Quarterly Review*, vol. 28, 2008, pp. 57–74.
- [10] S. Yoshidomi, J. Furukawa, M. Hasumi, and T. Sameshima, Mechanical stacking multi junction solar cells using transparent conductive adhesive, *Energy Procedia*, vol. 60, pp. 116–122, 2014.
- [11] Y. Vorobiev, P. Vorobiev, P. Horley, and J. González-Hernández, Experimental and theoretical evaluation of the solar energy collection by tracking and non-tracking photovoltaic panel, Proceedings of 2005 Solar World Congress (ISBN-0-89553-177-1), Orlando, FL, USA, August 6–12, 2005.
- [12] P. Vorobiev, and Y. Vorobiev, Automatic Sun tracking solar electric systems for applications on transport, Proceedings of 7th International Conference CCE 2010, Chiapas, Mexico, September 8–10 2010, pp. 66–70.
- [13] Y. Vorobiev, J. González-Hernández, P. Vorobiev, and L. Bulat, Thermal-photovoltaic solar hybrid system for efficient solar energy conversion, *Solar Energy*, vol. 80, pp. 170–176, 2006.
- [14] E. A. Chávez-Urbiola, Y. V. Vorobiev, and L. P. Bulat, Solar hybrid systems with thermoelectric generators, *Solar Energy*, vol. 86, pp. 369–378, 2012.
- [15] G. Hodes, Semiconductor and ceramic nanoparticle films deposited by chemical bath deposition. A review, *Physical Chemistry Chemical Physics*, vol. 9, pp. 2181–2196, 2007.
- [16] M. G. Sandoval-Paz, and R. Ramírez-Bon, Analysis of the early growth mechanisms during the chemical deposition of CdS thin films by spectroscopic ellipsometry, *Thin Solid Films*, vol. 517, pp. 6747–6752, 2009.
- [17] H. E. Esparza-Ponce, J. Hernández-Borja, A. Reyes-Rojas, M. Cervantes-Sánchez, Y. V. Vorobiev, R. Ramírez-Bon, J. F. Pérez-Robles, and J. González-Hernández, Growth technology, X-ray and optical properties of CdSe thin films, *Materials Chemistry and Physics*, vol. 113, pp. 824–828, 2009.

- [18] R. Ochoa-Landín, J. Sastre-Hernández, O. Vigil-Galán, and R. Ramírez-Bon, Chemically deposited CdS by an ammonia-free process for solar cells window layers, *Solar Energy*, vol. 84, pp. 208–214, 2010.
- [19] A. L. Salas-Villaseñor, I. Mejía, J. Hovarth *et al.*, Impact of gate dielectric in carrier mobility in low temperature chalcogenide thin film transistors for flexible electronics, *Electrochemical and Solid State Letters*, vol. 13, pp. H313–H316, 2010.
- [20] J. Hernandez Borja, Y. V. Vorobiev, and R. Ramirez Bon, Thin film solar cells of CdS/PbS chemically deposited by an ammonia-free process, *Solar Energy Materials and Solar Cells*, vol. 95, pp. 1882–1888, 2011.
- [21] R. S. Mane, and C. D. Lokhande, Chemical deposition method for metal chalcogenide thin films, *Materials Chemistry and Physics*, vol. 65, p. 1, 2000.
- [22] C. E. Pérez-García, R. Ramírez-Bon, and Y. V. Vorobiev, PbS thin films growth with CBD and PCBD techniques: a comparative study, *Chalcogenide Letters*, vol. 12, pp. 579–588, 2015.
- [23] H. Lima-Lima, and O. Portillo-Moreno, Análisis de reacciones en la transición de CdS (semiconductor) a CdCO₃ (aislante) en formato de películas delgadas obtenidas mediante DBQ, *Superficies Y Vacío*, vol. 21, p. 21, 2008.
- [24] I. R. Chávez-Urbiola, R. Ramírez Bon, and Y. V. Vorobiev, The transformation to cadmium oxide through annealing of cadmium oxide hydroxide deposited by ammonia-free SILAR method and the photocatalytic properties, *Thin Solid Films*, vol. 592, pp. 110–117, 2015.
- [25] I. R. Chávez-Urbiola, J. A. Bernal Martínez, J. Hernandez Borja, C.E. Perez Garcia, R. Ramírez Bon, and Y. V. Vorobiev, Combined CBD-CVD technique for preparation of II–VI semiconductor films for solar cells, *Energy Procedia*, vol. 57, pp. 24–31, 2014.
- [26] I. R. Chávez-Urbiola, J. A. Bernal Martínez, V. P. Makhniy, R. Ramírez Bon, and Y. V. Vorobiev, Preparation of II–VI and IV–VI semiconductor films for solar cells by the isovalent substitution technique with a CBD-made substrate, *Inorganic Materials*, vol. 50, pp. 546–550, 2014.
- [27] Datasheets for GaP photodiodes G1961, G1962 and G1963 produced by Hamamatsu, product catalog. <http://www.hamamatsu.com/us/en/products/category>
- [28] R. G. Dhere *et al.*, Development of substrate structure CdTe photovoltaic devices with performance exceeding 10%, *Proceedings of 38th IEEE PVSC*, pp. 3208–3211, 2012.
- [29] Internet data. <http://energy.gov/eere/sunshot/cadmium-telluride>
- [30] G. C. Rodrigues, P. Indelicato, J. P. Santos, P. Patté, and F. Parente, Systematic calculation of total atomic energies of ground state configurations, *Atomic Data and Nuclear Data and Tables*, vol. 86, pp. 117–233, 2004.

- [31] J. Li, and S.-H. Wei, Alignment of isovalent impurity levels: oxygen impurity in II–VI semiconductors, *Physical Review B*, vol. 73, 041201-1-4, 2006.
- [32] I. M. Dharmadasa, Review of the CdCl₂ treatment used in CdS/CdTe thin film solar cell development and new evidence towards improved understanding, *Coatings*, vol. 4, pp. 282–307, 2014.
- [33] T. Schmeyer, J. Fritsche, A. Thiben *et al.*, Effect of in situ UHV CdCl₂-activation on the electronic properties of CdTe thin film solar cells, *Thin Solid Films*, vol. 431–432, 84–89, 2003.

IntechOpen

